Pure Appl. Geophys. 172 (2015), 2635–2642

DOI 10.1007/s00024-015-1035-8

Pure and Applied Geophysics

# Shear Senses and Viscous Dissipation of Layered Ductile Simple Shear Zones

Kieran F. Mulchrone[1] and Soumyajit Mukherjee[2]

*Abstract*—Velocity profiles and shear heat profiles for inclined, layered Newtonian simple shear zones are considered. Reverse fault-like simple shear of the boundaries and upward net pressure gradient act together in such shear zones. As the velocity of the boundary increases, the point of highest velocity shifts from the lower layer of less viscosity into the upper layer. The shear heat profile shows a temperature peak inside the lower layer. For a more viscous upper layer, the point of highest velocity is located inside the upper layer and shifts towards the upper boundary of the shear zone. The shear heat profile shows a maximum temperature within the upper layer. Depending on the flow parameters of the two layers, the slip rate of the boundary, and the dip and thickness of the shear zone, a shear sense in reverse to the relative movement of the shear zone boundaries may develop. These models can decipher thermo-kinematics of layered shear zones in plate-scale hot orogens.

**Key words:** Ductile shear zones, shear sense, shear heat, Newtonian fluid, simple shear, Poiseuille flow.

## 1. Introduction

Ductile simple shear zones in rocks involve very slow movements parallel to their boundaries (Twiss and Moores 2007), with rates of a few millimeters per year (mm year$^{-1}$ ) or even less and develop sigmoid S-fabrics bound by primary shear C-planes (Berthé *et al.* 1979; Mukherjee 2011). High strain shear zones developed in polymineralic rocks segregate into layers of different mineralogies (e.g., Nicolas 1992; Jousselin *et al.* 2012; Montesi 2013; Shields *et al.* 2014). Ductile shear zones most commonly consist of relatively less deformed quartzofeldspathic bands alternated with intensely sheared mica layers (e.g., Figure 5.32c of Passchier and Trouw 2005; also see Druguet *et al.* 2009). Weaker/less competent layers equivalent to less viscous fluid in the ductile regime may develop due to inherent rock foliations where specific mineral aggregates occupy different layers (Altenberger 1997; Lister and Williams 1983; Passchier and Trouw 2005). In other cases, layer-parallel simple shear/Couette flow has been reported (Rhodes and Gayer 1978). Therefore, kinematics and shear heat/viscous dissipation in such layered shear zones in advanced stages of progressive deformation are not to be equated with those for shear zones with a single lithology modeled by many authors (e.g., Fleitout and Froideavaux 1980; Ramsay 1980; Mukherjee 2012; Mukherjee and Mulchrone 2013). This work furthers that of Mukherjee and Mulchrone (2013) to demonstrate the kinematics and shear heat related to layered, inclined simple shear zones. Understanding kinematics of (simple) shear zones is important to comprehend tectonics related to them (see Rosenberg and Handy 2000; Regenauer-lieb and Yuen 2003a, b).

## 2. The Model

### 2.1. Velocity Profiles

A shear zone with parallel, inclined rigid boundaries filled with two immiscible Newtonian fluids of different densities and viscosities is considered to undergo a top-to-up dip sense of simple shear (Fig. 1). The model consists of two layers, an upper layer (layer-1) with viscosity $\mu_1$, density $\rho_1$ and thickness $h_1$, and a lower layer (layer-2) with viscosity $\mu_2$, density $\rho_2$ and thickness $h_2$. We consider incompressible Newtonian rheology for both layers following a series of analytical and tectonic models that followed

[1] Department of Applied Mathematics, School of Mathematical Sciences, University College, Cork, Ireland.
[2] Department of Earth Sciences, Indian Institute of Technology Bombay, Powai, Mumbai 400 076, Maharashtra, India. E-mail: smukherjee@iitb.ac.in; soumyajitm@gmail.com

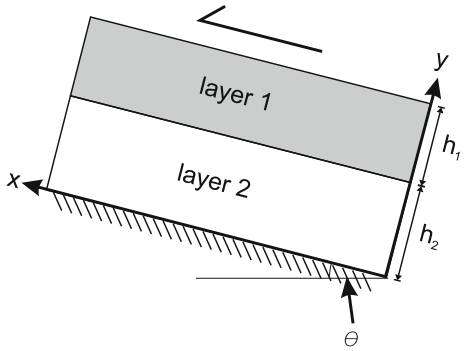


Figure 1
The inclined two-layer ductile shear zone. $\Theta$ Dip of shear zone. Thicknesses of layers 1 and 2 are $h_1$ and $h_2$, respectively

the same assumption (e.g., RAMBERG 1981; MUKHERJEE and MULCHRONE 2012 and references therein). Relative movement between the boundaries of the shear zone is modelled by considering the bottom boundary to be static, and the upper boundary to shear at a constant velocity ($U$) towards the up-dip direction. This is similar to reverse/thrust fault-like movement. In addition, as is prevalent in hot orogenic channels (e.g., RIVERS 2009), a pressure gradient ($\mathrm{d}p/\mathrm{d}x$) component is considered to push both layers in the up-dip direction and is counteracted by the weight of the fluids along the shear zone. This counteracting component is given by '$\rho_i g\sin\theta$' where $\rho_i$ is the density of the fluid, $g$ is the gravity, and $\theta$ is dip of the shear zone. Both fluids are considered to flow against gravity under net pressure gradients ($G_i = \mathrm{d}p/\mathrm{d}x - \rho_i g\sin\theta$). MUKHERJEE (2013a) modeled such extrusive flows to constrain the rheology of a Himalayan shear zone considering its single 'representative' lithology. In the present case, at the interface between the two layers, velocity ($u$) and shear stress ($\tau = \mu\frac{\mathrm{d}u}{\mathrm{d}y}$) become equal to satisfy the equation of motion (as in PAPANSTASIOU *et al*. 2000; POZRIKIDIS 2009). In other words, at their interface, two fluids stick together, attain a common velocity, and slip/faulting between them is not considered. This is the *'no slip boundary condition'* in fluid mechanics. MUKHERJEE (2012, 2013a, b) modelled the slow flow of a single extruding fluid along with shear at the boundary of the shear zone (BEAUMONT *et al*. 2001) as a simple shear since the distance between the two boundaries of the shear zone remain unchanged, and fluid particles translate parallel to the boundaries. We assume temperature change produced by shear to be insufficient to produce viscosity change in the two fluids.

The relevant equations are (TURCOTTE and SCHUBERT 2014):

$$\mu_1 \frac{\mathrm{d}^2 u_1}{\mathrm{d}y^2} = G_1 \tag{1}$$

$$\mu_2 \frac{\mathrm{d}^2 u_2}{\mathrm{d}y^2} = G_2 \tag{2}$$

Here $u_1$ is the velocity in layer-1 and $u_2$ is the equivalent in layer-2. The required boundary conditions for velocity are:

$$u_2(0) = 0;\ u_2(h_2) = u_1(h_2);\ u_1(h_1 + h_2) = U \tag{3}$$

and for shear stress equality they are:

$$\mu_1 \frac{\mathrm{d}u_1}{\mathrm{d}y}(h_2) = \mu_2 \frac{\mathrm{d}u_2}{\mathrm{d}y}(h_2) \tag{4}$$

Solving:

$$\begin{aligned} u_1(y) = {} & \frac{U}{a}\left(h_2(\mu_1 - \mu_2) + y\mu_2\right) \\ & + \frac{G_1}{2\mu_1}\left(y^2 - \frac{y}{\alpha}\left(2h_2\alpha + h_1^2 h_2\right)\right. \\ & \left. + \frac{h_2}{\alpha}(h_1 + h_2)(\alpha - h_1\mu_1)\right) \\ & + \frac{G_2 h_2^2}{2\alpha}(y - (h_1 + h_2)) \end{aligned} \tag{5}$$

$$u_2(y) = \frac{U\mu_1 y}{\alpha} - \frac{G_1 h_1^2 y}{2\alpha} + \frac{G_2 y}{2\mu_2}\left(y - \frac{h_2(\alpha + h_1\mu_2)}{\alpha}\right) \tag{6}$$

where

$$\alpha = h_1\mu_2 + h_2\mu_1. \tag{7}$$

The position of the maximum velocity in each layer can be obtained. In layer-1, the maximum, if existing, occurs at:

$$y = \frac{-2U\mu_1\mu_2 + G_1\left(2\alpha h_2 + h_1^2\mu_2\right) - G_2 h_2^2\mu_1}{2\alpha G_1} \tag{8}$$

In layer-2, the maximum, if existing, occurs at:

$$y = \frac{-2U\mu_1\mu_2 + G_1 h_1^2\mu_2 + G_2 h_2(\alpha + h_1\mu_2)}{2\alpha G_2} \tag{9}$$

The maximum velocity can occur in layer-1 only when $h_2 \le y \le h_1 + h_2$ and similarly the maximum

velocity for layer-2 can occur only for $0 \le y \le h_2$. First, for simplified algebraic representation, we define the following parameters:

$$\beta = \frac{G_2 h_2^2 \mu_1}{G_1 h_1^2},\ \gamma = \frac{-G_2 h_2^2 \mu_1 + G_1 h_1^2 \mu_2}{2\mu_1 \mu_2},$$
$$\delta = \frac{-2G_1 h_1 h_2 \mu_1 - G_2 h_2^2 \mu_1 - G_1 h_1^2 \mu_2}{2\mu_1 \mu_2}$$

Upon analysis, a maximum velocity occurs in layer-1 when any of the following conditions are satisfied:

1. $0 < \mu_2 < \beta,\ \gamma \le U \le \delta$
2. $\mu_2 = \beta,\ \gamma < U \le \delta$
3. $\mu_2 > \beta,\ 0 < U \le \delta$

However a maximum velocity occurs in layer-2 if:

4. $0 < \mu_2 < \beta,\ 0 < U \le \gamma$

This effectively implies that a maximum velocity occurs either in one layer or the other but not in both layers simultaneously. Two examples of velocity profiles are presented in Fig. 2. Starting with a passive linear marker perpendicular to the boundaries, two dissimilar segments of parabolic velocity profiles develop inside the two fluids for $G_i > 0$ (profiles for $U = 1$–$9$ in Fig. 2a; Eqs. 5, 6). As expected, parabolic profiles also develop when both the boundaries remain static, i.e., $U = 0$, yet a pressure gradient extrudes both the fluids, i.e., $G_i > 0$ (bottommost curve in Fig. 2a). In Fig. 2a, $h_2 > h_1,\ \mu_1 > \mu_2,\ G_1 > G_2$ and the critical parameters are: $\beta = 24,\ \gamma = 5.75,\ \delta = 8.25$. In this case, $\mu_2 < \beta$, hence condition-1 above may apply. As $U$ varies from 0 to 5, condition 4 applies and the maximum velocity occurs in layer-2. When $U$ ranges from 6 to 8, condition 1 applies and the maximum velocity occurs within layer-1. For $U = 9$, the maximum velocity is attained where layer-1 touches the upper boundary of the shear zone. In Fig. 2b, $h_1 > h_2,\ \mu_2 > \mu_1,\ G_2 > G_1$ and critical parameters: $\beta = 0.08, \gamma = -5.9, \delta = 7.3$. In this case, $\mu_2 > \beta$ and condition 3 applies. A maximum velocity occurs in layer-1 while $U \le \delta$. Hence, a maximum velocity for $U = 8$ or 9 occurs where layer-1 touches the upper boundary of the shear zone.

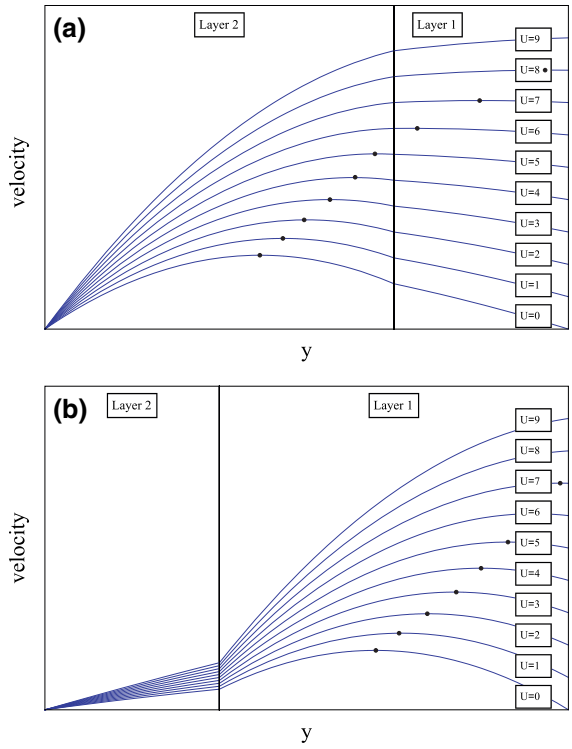


Figure 2
Velocity profiles: **a** for: $h_2 > h_1,\ \mu_1 > \mu_2,\ G_1 > G_2$; critical parameters: $\beta = 24,\ \gamma = 5.75,\ \delta = 8.25$; **b** for: $h_1 > h_2,\ \mu_2 > \mu_1,\ G_2 > G_1$; critical parameters: $\beta = 0.08,\ \gamma = -5.9,\ \delta = 7.3$. *Dots on profiles* points of highest velocities. $U$ velocity of shear of the *upper boundary* of the shear zone: shown in Fig. 1

Depending on (1) the algebraic relation amongst the flow parameters (density, viscosity, net pressure gradient) of the two layers, on (2) the slip rate of the boundary, and dip and thickness of the shear zone, and, (3) for a layer-1 thinner and more viscous than layer-2, the maximum velocity attained within the shear zone can fall inside either layer-2 (for $U = 1$–$5$ in Fig. 2a), layer-1 (for $U = 6$–$8$ onwards in Fig. 2a), or at the contact between layer-1 and the upper boundary of the shear zone ($U = 9$ in Fig. 2a). Since the bottom boundary was considered static, velocity profiles ($U = 0$–$7$ in Fig. 2a) in various cases for layer-2 in contact with the boundary of the shear zone display no movement. When both the boundaries remain static, obviously, the velocity profile touches the two end points of the y-axis (case $U = 0$ in Fig. 2a). The ductile shear sense reverses across the point of maximum velocity in the velocity profile if it

falls inside the shear zone (cases $U = 1$–$8$ in Fig. 2a, and $U = 1$–$6$ in Fig. 2b). If the point falls on the boundary of the shear zone (cases $U = 9$ in Fig. 2a and $U = 7$–$9$ in Fig. 2b), then a uniform shear sense develops within the shear zone.

In both cases, the chosen parameters were such that the parabolic segments in layer-1 in Fig. 2a and those in layer-2 in Fig. 2b resemble straight lines opon a cursory observation. In reality, those are segments of parabolas of low curvatures. A uniform ductile shear sense develops in those layers for various slip rates (i.e., for various $U$ values).

### 2.2. *Shear Heat Profiles*

Following Lautrup (2011) and Mukherjee and Mulchrone (2013), the temperature ($T$) distribution in the steady state is governed by the following general equation in layer-1 (temperature $T_1$, $h_2 \leq y \leq h_1 + h_2$):

$$k\frac{\mathrm{d}^2 T_1}{\mathrm{d}y^2} + \mu_1\left(\frac{\mathrm{d}u_1}{\mathrm{d}y}\right)^2 = 0 \qquad (10)$$

In layer-2 (temperature $T_2$, $0 \leq y \leq h_2$):

$$k\frac{\mathrm{d}^2 T_2}{\mathrm{d}y^2} + \mu_2\left(\frac{\mathrm{d}u_2}{\mathrm{d}y}\right)^2 = 0 \qquad (11)$$

Boundary conditions are $T_2(0) = T_1$, $T_1(h_1 + h_2) = T_u, T_1(h_2) = T_2(h_2)$ and heat flux equality at the boundary between the layers:

$$k\frac{\mathrm{d}T_1}{\mathrm{d}y}(h_2) = k\frac{\mathrm{d}T_2}{\mathrm{d}y}(h_2) \qquad (12)$$

where $T_\mathrm{l}$ and $T_\mathrm{u}$ are the temperatures at the lower and upper boundaries of the shear zone, respectively. These equations are readily solved, and the resulting equations, owing to their length, are displayed in the "Appendix". The temperature profile due to shear heating is illustrated in Fig. 3 for the parameters used in the discussed velocity profile. In addition, the temperature at the lower and upper boundary is set to zero so that only the temperature due to shear heating is plotted.

Figure 3a presents a shear heat/viscous dissipation profile in the bi-viscous shear zone for the case of Fig. 2a. Here, when both the boundaries are static, i.e., $U = 0$, the shear heat profile is almost bell-shaped, indicating a broad zone of higher temperatures at the central portion of the shear zone. With an increasing slip rate ($U = 0$–$9$), the point of maximum temperature developed inside layer-2 shifts towards the fluid interface.

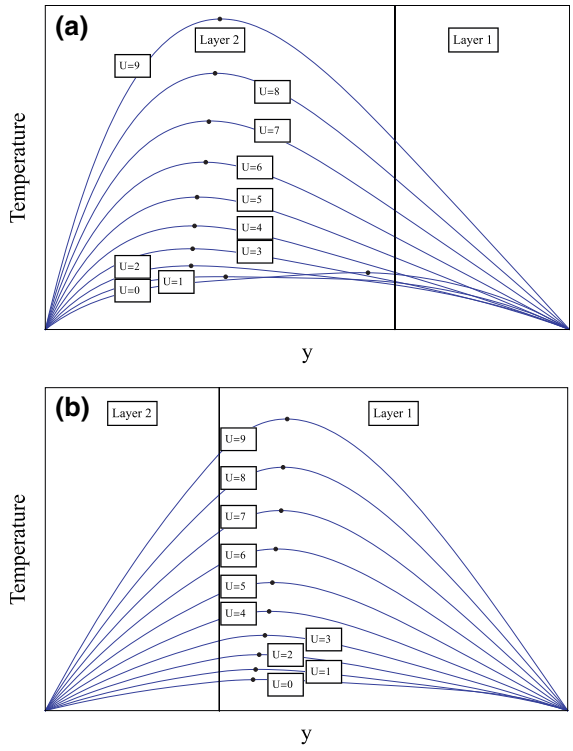


Figure 3
Temperature profiles corresponding to the parameters as stated in caption of Fig. 2. *Dots on profiles* indicate points of highest temperatures. $U$ velocity of shear of the *upper boundary* of the shear zone: shown in Fig. 1

Figure 3b presents a shear heat/viscous dissipation profile in the doubly viscous shear zone for the case of Fig. 2b. The combination of flow parameters in both the layers are such that an increase in shear rate $U$ (from 0 to 9) progressively creates a more intense temperature maximum inside layer-1 closer to the fluid interface. However, unlike the case of Fig. 3a, an increase in $U$ does not relocate the point of maximum temperature significantly.

Notice that, obviously, velocity profiles and shear heat profiles do not match geometrically (compare Figs. 2a with 3a, 2b with 3b). In both cases (Fig. 3a, b), no shear heat is produced at the boundaries of the shear zone. In addition, when all the other parameters remain constant, an increase in slip rate increases the

shear heat. These conclusions in one way match with univiscous shear zones in terms of (1) the location of shear heat development, and (2) the relationship between slip rate of the boundary and shear heat (Mukherjee and Mulchrone 2013). Shear heat has been deciphered from field data (Starin *et al*. 2000) and has been described by analytical models (e.g., Turcotte and Schubert 2014). Extending the concept of shear heat to multi-layered sequences with 'n' layers, we can say that two shear senses may develop under coeval extrusive flow and simple shear of shear zone boundaries. If we consider that the d$p$/d$x$ component does not exist in the natural shear zone, the present work still remains valid. In that case, we need consider $G_i = -\rho_i g \sin\theta$ in the beginning to get the velocity and the shear heat profiles. Considering a set of realistic magnitudes for a biviscous shear zone: $\theta = 45°$, $G_1 = 1$ kbar km$^{-1}$, $G_2 = 3 \times 10^5$ kbar km$^{-1}$, $U = 2$ mm year$^{-1}$, $h_1 = 2$ km, $h_2 = 4$ km, $k_1 = 4.2$ W m K$^{-1}$, $k_2 = 2.1$ W m K$^{-1}$, and $\mu_1 = \mu_2 = 10^{21}$ P, a $T_{max} = 62$ °C is attained within layer-2. On the other hand, taking $\mu_1 = 10^{21}$ P and $\mu_2 = 10^{22}$ P and all other parameters to be the same, $T_{max} = 200$ °C develops within layer-2.

## 3. Applicability

Deformation in shear zones, where Poiseuille flow and ductile shear work together, as in the present case, has been modeled as Newtonian fluid flow (Warren *et al*. 2008a, b, c), and especially for molten granites and creep of ultra-high pressure rocks by dissolution precipitation and granular flow (Mukherjee and Mulchrone 2012). Strictly speaking, (1) if the sizes of mineral grains remain the same during ductile deformation, and/or (2) for very slow deformation as in the geological cases, the deformation can be approximated as Newtonian fluid flow (Hobbs 1972). The first condition seems unlikely in natural ductile shear zones (see Mukherjee 2013b, 2014). It has been argued that some shear zones reaching the mantle (Pili *et al*. 1997) can be Newtonian (Ranalli 1984).

The biviscous model elaborated here ignores many complicated details of shear zones such as the effects of geothermal gradient (such as temperature and, hence, depth dependence of density and viscosity), the feedback between viscosity and shear heat, curved (Mukherjee and Biswas 2014) and/or non-parallel shear zone boundaries (Mandal *et al*. 2002), gravitational spreading and/or erosion of the extruded mass, partial melting, volume change/compressible rheology, strain localization, the occurrence of pure shear, i.e., widening/narrowing of the shear zone (e.g., Xypolias 2010), and grain growth, etc. The present model assumes immiscible Newtonian viscous fluids to represent layers within rocks, and is quite unlike two-phase materials under deformation where one of the phases is an inclusion within the other (Vigneresse 2004). Shear zones can also have diffuse boundaries (Díaz Azpiroz and Fernández 2005), and contacts between different rock types may not be perfectly linear nor accurately parallel to the shear zone boundaries. For ductile shear zones consisting of pinch and swell structures, mullions (review in Hudleston and Lan 1993), microboudins (Masuda and Kimura 2004), mylonites (Chen *et al*. 2014), and containing folds of quite different styles/very high cylindricity (Hudleston and Treagus 2010), the rheology and has been interpreted to be non-Newtonian. In such shear zones, the models presented here would not fit. Crustal ductile shear zones at shallow depth are heterogeneous (e.g., Vitale and Mazzoli 2008, 2015) and are not to be modeled in the way this work did.

## 4. Discussions

### 4.1. Small-Scale Context

An alternation of quartzo-feldspathic and mica layers occurs in ductile shear zones at the cm and mm scale. The quartzo-feldspathic layers have a density $\rho = 2{,}630$–$2{,}650$ kg m$^{-3}$ (that of quartz and albite) and a thermal conductivity $k = 2.2$–$8.4$ W m K$^{-1}$ (that of orthoclase, albite, microcline, anorthite, quartz and quartzite). On the other hand, mica-rich layers have $\rho = 2{,}790$–$3{,}050$ kg m$^{-3}$ (that of biotite, muscovite, phlogopite) and a $k = 1.9$–$4.9$ W m K$^{-1}$ (that of biotite, muscovite, talc, chlorite; Henderson and Henderson 2009). Depending on the anisotropy/imperfection in minerals and pressure–temperature conditions, the thermal conductivity can vary further. Thus, variations in '$\rho$' and '$k$' in such layers during

ductile deformation is expected to develop behaviour like that shown in Fig. 2a and b.

### 4.2. Regional Context

In the Greater Himalayan Crystallines, the net pressure gradient '$G_i$' has been reported to range from 0.20 to 6 kbar km$^{-1}$ (reviewed in Mukherjee 2013a). Crustal Poiseuille flow of a single fluid along with shear of the boundary has been inferred in a few 'hot' orogens such as the Andes (Rivers 2009). For example, the total slip rate of the lower and the upper boundaries of the Greater Himalayan Crystallines, i.e., the Main Central Thrust and the South Tibetan Detachment System, respectively, were reported to be as high as 0.7–131 mm year$^{-1}$ within their periods of activation. The Greater Himalayan Crystallines complex is 6–58 km thick, ranges in density from 2,200 to 3,100 kg m$^{-3}$ and has a viscosity within $10^{17}$–$10^{24}$ P (Mukherjee 2013a). However, recent field-studies considered the Greater Himalayan Crystallines to consist of two layers parallel to its boundaries: the lower non-migmatitic schists of various metamorphic grades, and the upper migmatitic layer, presumably less viscous (Mukherjee 2010, 2013a; Larson *et al.* 2010). The timing of development of the different grades of metamorphism within the schist has not been constrained (Yin 2006). However, Himalayan geologists assume implicitly that they were coeval. Secondly, as the amphibolite and greenschist facies schists are not layered, the present study cannot create finer models suitable for the prototype. In addition, the timing of the contact between schists and migmatites is not constrained in the Himalayan geological literature (Yin 2006; Mukherjee 2013a).

Simultaneous reverse ductile shear has been established geochronologically for the Greater Himalayan Crystallines (Godin *et al.* 2006): top-to-S/SW shear from the Main Central Thrust and top-to-N/NE from the South Tibetan Detachment System around the mid-Miocene period. This is similar to the presented case in which reverse ductile shear occurs within two-layered shear zones (Fig. 2a, b).

Density and viscosity of migmatities range from 2.8–3.1 gm cm$^{-3}$ and $10^{17}$–$10^{21}$ P, respectively. In schists they range from 2.4–2.9 gm cm$^{-3}$ and $10^{19}$–$10^{20}$ P, respectively (Table 1 of Mukherjee 2013a). Ductile shear in the two-layered Greater Himalayan Crystallines happened during migmatization of the upper layer during the mid-Miocene (Godin *et al* 2006; Yin 2006). Therefore, the density difference mentioned between the schists and the migmatites holds true.

It can finally be concluded that the present two-layer ductile shear zone can help achieve a better understanding of shear senses and shear heat. Taking '$G_i$' $< 0$ and $U = 0$, it can be applied to predict kinematics and shear heat profiles of layered subduction channels (Warren *et al.* 2008b).

### Acknowledgments

Department of Science and Technology's (New Delhi) satellite project: *IR/S4/ESF-16/2009(G)* supported SM. Thanks to two anonymous reviewers for critical comments, Eugenio Carminati for editorial handling and reviewing, Rakesh Biswas for discussions, and Priyanka Ganesh for assistance.

### Appendix

Solutions of Eq. (12): shear heat profile for layer-1 and 2:

$$
\begin{aligned}
T_1(y) = {} & \frac{1}{24k(h_1+h_2)\mu_1\mu_2(h_2\mu_1+h_1\mu_2)^2} \\
& \times \left(-G_2^2h_2^4(-y+h_1+h_2)\mu_1(h_2^2\mu_1(\mu_1-3\mu_2))\right. \\
& + 3yh_2\mu_1\mu_2 + h_1\mu_2(3y\mu_1+2h_1\mu_2)) \\
& + 2G_2(y-h_1-h_2)h_2^2\mu_1\mu_2(2U\mu_1(h_2^2(\mu_1 \\
& - 3\mu_2) + 3yh_1\mu_2 + (3y-2h_1)h_2\mu_2) \\
& + G_1(2(y-h_2)^2h_2^2\mu_1 - h_1^3(y-2h_2)\mu_2 \\
& + h_1^2(yh_2(2\mu_1-5\mu_2) - h_2^2(\mu_1-3\mu_2) \\
& + 2y^2\mu_2) + 2h_1(y-h_2)h_2(y\mu_1+(y-h_2)\mu_2))) \\
& + \mu_2(4UG_1(y-h_1-h_2)\mu_1\mu_2(2(y-h_2)^2h_2^2\mu_1 \\
& - yh_1^3\mu_2 + h_1^2(2y-3h_2)(h_2(\mu_1-\mu_2)+y\mu_2) \\
& + 2h_1(y-h_2)h_2(y\mu_1(y-h_2)\mu_2)) - 12\mu_1 \\
& \times (h_1(-2kh_1^2T_l - U^2y^2\mu_1 + yh_1(2kT_l - 2kT_u
\end{aligned}
$$

$$
\begin{aligned}
&+ U^2\mu_1))\mu_2^2 + h_2^3\mu_1(-2KT_l\mu_1 + U^2(\mu_1\\
&- \mu_2)\mu_2) - h_2\mu_2(U^2y^2\mu_1\mu_2 + 2kh_1^2T_l(2\mu_1\\
&+ \mu_2) - 2yh_1\mu_1(2kT_l - 2KT_u + U^2\mu_2))\\
&+ h_2^2\mu_1(-2kyT_u\mu_1 + U^2\mu_2((-y + h_1)\mu_1\\
&+ (2y - h_1)\mu_2) + 2kT_l((y - h_1)\mu_1 - 2h_1\mu_2)))\\
&+ G_1^2(y - h_1 - h_2)(2(y - h_2)^3h_2^3\mu_1^2\\
&+ 2h_1(y - h_2)^2h_2^2\mu_1(y\mu_1 + 2(y - h_2)\mu_2)\\
&+ h_1^4\mu_2(3h_2^2(\mu_1 - \mu_2) - 2y^2\mu_2 + 5yh_2\mu_2\\
&+ 2h_1^2(y - h_2)h_2(y^2\mu_2(2\mu_1 + \mu_2) + h_2^2\mu_2(2\mu_1\\
&+ \mu_2) + yh_2(\mu_1^2 - 4\mu_1\mu_2 - 2\mu_2^2)) + 2h_1^3(y^3\mu_2^2\\
&- 4y^2h_2\mu_2^2 - 2h_2^3\mu_2^2 + yh_2^2(\mu_1^2 + 5\mu_2^2)))))
\end{aligned}
$$

$$
\begin{aligned}
T_2(y) = &\frac{1}{24k(h_1 + h_2)\mu_1\mu_2(h_2\mu_1 + h_1\mu_2)^2}\\
&\times (yG_2^2\mu_1(-h_2^3(-2y^3 + 4y^2h_2 - 3yh_2^2\\
&+ h_2^3)\mu_1^2 + 2h_1^3(y^3 - 4y^2h_2 + 6yh_2^2 - 4h_2^3)\mu_2^2\\
&+ h_1h_2^2\mu_1((2y^3 - 4y^2h_2 + 3yh_2^2 - 2h_2^3)\mu_1\\
&+ 4(y - h_2)^3\mu_2) + h_1^2h_2\mu_2((4y^3 - 12y^2h_2\\
&+ 12yh_2^2 - 7h_2^3)\mu_1 + 2(y^3 - 4y^2h_2 + 6yh_2^2\\
&- 3h_3^2)\mu_2)) - 2yG_2\mu_1\mu_2(-2U\mu_1(h_2^2(2y^2\\
&- 3yh_2 + h_2^2)\mu_1 + h_1^2(2y^2 - 6yh_2 + 3h_2^2)\mu_2\\
&+ h_1h_2(y(2y - 3h_2)\mu_1 + 2(y^2 - 3yh_2\\
&+ 2h_2^2)\mu_2)) + G_1h_1^2(h_2^2(2y^2 - 3yh_2 + h_2^2)\mu_1\\
&+ h_1^2(2y^2 - 6yh_2 + 5h_2^2)\mu_2 + h_1h_2((2y^2\\
&- 3yh_2 + 2h_2^2)\mu_1 + 2(y^2 - 3yh_2 + 2h_2^2)\mu_2)))\\
&+ \mu_2(-4UyG_1h_i^2\mu_1\mu_2(h_1(3y - 4h_2)\mu_1\\
&+ 3(y - h_2)h_2\mu_1 - h_1^2\mu_2) + yG_1^2h_1^4(3(y\\
&- 2h_1)h_2\mu_1\mu_2 - h_2^2\mu_1(2\mu_1 + 3\mu_2)\\
&+ h_1\mu_2(3y\mu_1 - h_1\mu_2)) - 12\mu_1(-2kh_3^2T_l\mu_1^2\\
&+ h_1\mu_2(-U^2y^2\mu_1^2 - 2kh_1((-y + h_1))T_l\\
&+ yT_u)\mu_2 + U^2yh_1\mu_1\mu_2) - h_2\mu_2(U^2y^2\mu_1^2\\
&- 2yh_1\mu_1(2kT_l - 2kT_u + U^2\mu_1)\\
&+ 2kh_1^2T_l(2\mu_1 + \mu_2)) + h_2^2\mu_1(y\mu_1(-2kT_u\\
&+ U^2\mu_2) + 2kT_l((y - h_1)\mu_1 - 2h_1\mu_2)))))
\end{aligned}
$$

## References


Altenberger, U. (1997), *Strain localization mechanisms in deep-seated layered rocks.* Geol. Rund. *86* 56–68.

Beaumont, C., Jamieson, R.A., Nguyen, M.H. and Lee, B. (2001), *Himalayan tectonics explained by extrusion of a low-viscosity crustal channel coupled to focused surface denudation.* Nature *414*, 738–742.

Berthé, D., Choukroune, P., Jegouzo, P. (1979), *Orthogneiss, mylonite and non-coaxial deformation of granites: the example from the south Armorican shear zone.* J. Struct. Geol. *1*, 31–42.

Chen, Y., Ziang, D., Zhu, G. and Xiang, B. (2014), *The formation of micafish: A modelling investigation based on micromechanics.* J. Struct. Geol. *68*, 300–315.

Díaz Azpiroz, M. and Fernández, C. (2005), *Kinematic analysis of the southern Iberian shear zone and tectonic evolution of the Acebuches metabasites (SW Variscan Iberian Massif).* Tectonics *24*, TC3010.

Druguet, E., Alsop, G.I. and Carreras, J. (2009), *Coeval brittle and ductile structures associated with extreme deformation partitioning in a multilayer sequence.* J.Struct. Geol. *31*, 498–511.

Fleitout, L. and Froideavaux, C. (1980), *Thermal and mechanical evolution of shear zones.* J. Struct. Geol. *2*, 159–164.

Godin, L., Grujic, D., Law, R.D. and Searle, M.P. (2006), *Channel flow, extrusion and extrusion in continental collision zones: an introduction. In: Law RD, Searle MP (eds) Channel flow, extrusion and extrusion in continental collision zones.* Geol. Soc. Lond. Spec. Publ. *268*, 1–23.

Henderson, P., Henderson, G.M. (2009), *The Cambridge Handbook of Earth Science Data.* Cambridge University Press. pp. 65–67.

Hobbs, B.E. (1972), *Deformation of non-Newtonian materials in simple shear. Flow and fracture of rocks.* (H.C. Heard, I.Y. Borg, N.L. Carter and B.C. Raleigh, eds) Am. Geophys. Union, Geophys. Monograph *16*, 243–258.

Hudleston, P.J. and Lan, L. (1993), *Information from fold shapes.* J. Struct. Geol. *15*, 253–264.

Hudleston PJ, Treagus SH. (2010), *Information from folds: A review*. J. Struct. Geol. *32*, 2042–2071.

Jousselin, D., Morales, L.F.G., Nicolle, M. and Stephent A. (2012), *Gabbro layering induced by simple shear in the Oman ophiolite Moho transition zone*. Earth Planet. Sci. Lett. 331–332, 55–66.

Larson, K.P., Godin, L. and Price, R.A. (2010), *Relationships between displacement and distortion in orogens: linking the Himalayan foreland and hinterland in central Nepal.* Geol. Soc. Am. Bull. *122*, 1116–1134.

Lautrup, B. (2011), *Physics of continuous matter.* Second Edition. Taylor & Francis. p. 381.

Lister, G.S. and Williams, P.F. (1983), *The partitioning of deformation in flowing rock masses.* Tectonophysics *92*, 1–33.

Mandal, N., Samanta, S.K. and Chakraborty, C. (2002), *Flow and strain patterns at the terminations of tapered shear zones.* J. Struct. Geol. *24*, 297–309.

Masuda, T. and Kimura, N. (2004), *Can a Newtonian viscous-matrix model be applied to microboudinage of columnar grains in quartzose tectonites?* J. Struct. Geol. *26*, 1749–1754.

Montesi, L.G.T. (2013), *Fabric development as the key for forming ductile shear zones and enabling plate tectonics.* J. Struct. Geol. *50*, 254–266.

Mukherjee, S. (2010), *Structures at Meso- and Micro-scales in the Sutlej section of the Higher Himalayan Shear Zone in Himalaya*. e-Terra *7*, 1–27.

Mukherjee, S. (2011), *Mineral fish: their morphological classification, usefulness as shear sense indicators and genesis*. Int. J. Earth Sci. *100*, 1303–1314.

Mukherjee, S. (2012), *Simple shear is not so simple! Kinematics and shear senses in Newtonian viscous simple shear zones.* Geol. Mag. *149*, 819–826.

Mukherjee, S. (2013a), *Channel flow extrusion model to constrain dynamic viscosity and Prandtl number of the Higher Himalayan Shear Zone*. Int. J. Earth Sci. *102*, 1811–1835.

Mukherjee, S. (2013b), *Deformation Microstructures in Rocks.* Springer.

Mukherjee, S. (2014), *Atlas of shear zone structures in meso-scale*. Springer.

Mukherjee, S. and Biswas, R. (2014), *Kinematics of horizontal simple shear zones of concentric arcs (Taylor–Couette flow) with incompressible Newtonian rheology.* Int. J. Earth Sci. *103*, 597–602.

Mukherjee, S. and Mulchrone, K.F. (2012), *Estimating the viscosity and Prandtl number of the Tso Morari crystalline gneiss dome, Indian western Himalaya*. Int. J. Earth Sci. *101*, 1929–1947.

Mukherjee, S. and Mulchrone, K.F. (2013), Viscous dissipation pattern in incompressible Newtonian simple shear zones: an analytical model. Int. J. Earth Sci. 102, 1165–1170.

Nicolas, A. (1992), *Kinematics in magmatic rocks with special reference to gabbros*. J. Petrol. *33*, 891–915.

Passchier, C.W. and Trouw, R.A.J. (2005), *Microtectonics*. Springer. Second Edition. Berlin.

Papanstasiou, C.T., Georgioi, G.C. and Alexandrou, A.N. (2000), *Viscous Fluid Flow*. Florida: CRC Press.

Pili, E., Ricard, Y., Lardeaux, J.-M. and Sheppard, S.M.F. (1997), *Lithospheric shear zones and mantle-crust connections*. Tectonophysics *280*, 15–29.

Pozrikidis, C. (2009), *Fluid dynamics: Theory, Computation, and Numerical Simulation*. Second Edition, Springer, New York, pp. 360–424.

Ramberg, H. (1981), *Gravity, deformation and the Earth's crust in theory, experiments and geological applications.* 2nd edn. Academic Press, London.

Ramsay, J.G. (1980), *Shear zone geometry: a review*. J. Struct. Geol. **2**, 83–99.

Ranalli, G. (1984), *On the possibility of Newtonian flow in the upper mantle*. Tectonophysics *108*, 179–192.

Regenauer-lieb, K. and Yuen, D.A. (2003), *Modeling shear zones in geological and planetary sciences: solid- and fluid-thermal–mechanical approaches.* Earth Sci. Rev. *63*, 295–349.

Rivers, T. (2009), *The Grenville province as a large hot long-duration collisional orogen—insights from the spatial and thermal evolution of its orogenic fronts. Ancient Orogens and Modern Analogues.* (J.B. Murphy, J.D. Keppie, and A.J. Hynes, eds) Geol Soc, London, Spec Publ *327*, 405–444.

Regenauer-Lieb, K. and Yuen, D.A. (2003), *Modeling shear zones in geological and planetary sciences: solid-and fluid-thermal-mechanical approaches.* Earth Sci. Rev. *63*, 295–349.

Rhodes, S. and Gayer, R.A. (1978), *Non-cylindrical folds, linear structures in the X direction and mylonite developed during transtension of the Caledonian Kalak Nappe Complex of Finnmark*. Geol. Mag. *114*, 329–408.

Shields, J. K., Mader, H. M., Pistone, M., Caricchi, L., Floess, D.and Putlitz *B.* (2014), *Strain-induced outgassing of three-phase magmas during simple shear.* J. Geophys. Res. Solid Earth *119*, 6936–6957.

Starin, L., Yuen, D.A., Bergeron, S.Y. (2000), *Thermal evolution of sedimentary basin formation with variable thermal conductivity.* Geophys. Res. Lett. *27*, 265–268.

Rosenberg, C.L., Handy, M.R. (2000), *Syntectonic melt pathways during simple shearing of a partially molten rock analogue (Norcamphor-Benzamide)*. J. Geophys. Res. *105*, 3135–3149.

Turcotte, D. and Schubert, G. (2014), *Geodynamics*. Third Edition. Cambridge University Press.

Twiss, R.J. and Moores, E.M. (2007), *Structural Geology*. 2nd ed. New York: W. H Freeman and Company, 736 pp.

Vigneresse, J.L. (2004), *Rheology of a two-phase material with applications to partially molten rocks, plastic deformation and saturated soils. In: Flow Processes in Faults and Shear Zones.* (G.I. Alsop, R.E. Holdsworth and K.J.M. McCafrey, eds) Geol. Soc., London, Special Publication *224*, pp. 79–94.

Vitale, S. and Mazzoli, S. (2008), *Heterogeneous shear zone evolution: the role of shear strain hardening/softening*. J. Struct. Geol. *30*, 1363–1395.

Vitale, S. and Mazzoli, S. (2015), *From finite to incremental strain: insights into heterogeneous shear zone evolution. In: Mukherjee S, Mulchrone KF (Eds) Kinematics of Ductile Shear Zones in Meso- and Micro-scales*. Wiley Blackwell.

Warren, C.J., Beaumont, C. and Jamieson, R.A. (2008a), *Deep subduction and rapid exhumation: role of crustal strength and strain weakening in continental subduction and ultrahigh-pressure rock exhumation*. Tectonics *27*, TC6002.

Warren, C.J., Beaumont, C. and Jamieson, R.A. (2008b), *Modelling tectonic styles and ultra-high pressure (UHP) rock exhumation during the transition from oceanic subduction to continental collision.* Earth Planet. Sci. Lett. *267*, 129–145.

Warren, *C.J.,* Beaumont, C. and Jamieson, *R.A.* (2008c), *Formation and exhumation of ultra-high pressure rocks during continental collision: role of detachment in the subduction channel*. Geochem. Geophys. Geosys. *9*, Q04019.

Xypolias, P. (2010), *Vorticity analysis in shear zones: a review of methods and applications.* J. Struct. Geol. *32*, 2072–2092.

Yin, A. (2006), *Cenozoic tectonic evolution of the Himalayan orogen as constrained by along-strike variation of structural geometry, exhumation history, and foreland sedimentation*. Earth-Sci. Rev. *76*, 1–131.

(Received September 13, 2014, revised January 7, 2015, accepted January 8, 2015, Published online February 15, 2015)